Use of Active Material in Three-Level Solid State Masers*

By E. O. SCHULZ-DuBOIS, H. E. D. SCOVIL, and R. W. DeGRASSE

(Manuscript received January 2, 1959)

The three-level excitation method for solid state masers, including some background material on paramagnetic resonance, is reviewed. With respect to the experimental application of the maser material, two cases can be distinguished. In the first, maser action is based mainly on a favorable relaxation time ratio in signal and idler transitions. It is shown that the relaxation time ratio can be changed artificially by a doping technique. Experimental evidence is presented for two such doping techniques, one self-doping, the other impurity doping. In the second case, maser action is based primarily on a favorable frequency ratio of signal and idler transitions. Maser experiments using this approach are described. In addition, excitation of unidirectional gain and attenuation by circular polarization is discussed. Properties of practical isolator materials are surveyed; they include high-concentration paramagnetic and polycrystalline ferrimagnetic materials.

1. INTRODUCTION

In 1956, Bloembergen[1] proposed a three-level excitation scheme for obtaining microwave amplification by stimulated emission of radiation in paramagnetic solids, or three-level solid state *maser* (3LSSM) for short. It is superior to many other microwave amplifiers in that its noise contribution to an amplified signal should be virtually negligible compared to other noise sources in a system. The principal advantage of a solid state maser over a gaseous maser is that the amplified bandwidth should be of the order of megacycles, a magnitude sufficient for many communication applications. In contrast to the two-level solid state masers, its gain factor should be constant in time.

* This work was supported in part by the U. S. Army Signal Corps under Contract DA-36-039 sc-73224.

Experimental work has confirmed the theoretical predictions. It has been shown that microwave energy can be extracted from paramagnetics by stimulated emission.[2,3,4] If the circuit employed consists of a microwave resonant cavity, the energy extracted can be used to maintain either oscillations or amplification depending on the choice of the coupling parameter. Three paramagnetic salts have been used as active materials. These are gadolinium ethyl sulfate,[2] potassium chromicyanide[3] and ruby.[4] Gain and bandwidth obtained are in agreement with theoretical expectations. Noise measurements have indicated that maser noise is of the magnitude expected.

More recently, traveling wave masers (TWM) have been developed, as described in the accompanying paper.[5] A TWM is a transmission device which can be designed to be nonreciprocal. That is, power traveling from the input to the output is amplified while power traveling the opposite direction is attenuated. A nonreciprocal TWM offers several advantages over a cavity-type maser. Among these are greater gain stability, larger instantaneous bandwidth and the possibility of electronic tuning over a wider frequency range. Gain stability is of great practical importance because in many applications, gain fluctuations deteriorate the system's performance in the same way as noise.

In this paper, the active materials aspect of 3LSSM is treated. Viewpoints are presented on how a given paramagnetic spectrum can be used efficiently in maser applications. Two typical modes of operation are described for active maser materials. Properties of both are evaluated and illustrated by experimental results obtained with gadolinium ethyl sulfate and ruby. Also, those material aspects are discussed which are relevant to nonreciprocal behavior.

II. PARAMAGNETIC RESONANCE IN CRYSTALS

Consider a dilute concentration of paramagnetic ions placed in a diamagnetic host crystal. Obeying quantum laws, each ion can exist in one of several energy states. The number of such states is $2S + 1$, where S is the effective spin associated with the ion. The energy of any state stems from two contributions. One is Zeeman energy, that is, magnetostatic interaction of an applied magnetic field with the magnetic moment of unpaired electrons within the paramagnetic ion. The other is electrostatic in nature and leads to "zero field splitting", that is, separation of energy levels in the absence of an external magnetic field. This latter interaction takes place between the electrostatic field due to neighbors of the ion considered and the electronic charge present in the orbital states of the ion. It is apparent that this zero field energy will reflect

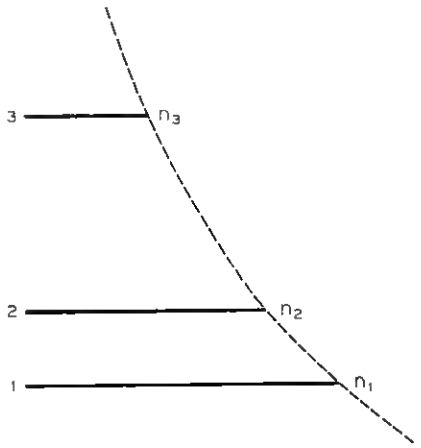

Fig. 1 — Three-level system in thermal equilibrium.

the geometry of the ion environment. As a rule, energy levels are about equally spaced if the magnetic energy outweighs the zero field energy. The spacing is rather unequal in the other extreme.

Fig. 1 shows a three-level scheme which may be part of a scheme of more levels. It is assumed that all three transitions between these are reasonably probable. This can be ascertained by calculations or, preferably, by direct observation of the transitions. A transition from E_i to E_j is excited by radiation of frequency $\nu_{ij} = (E_i - E_j)/h$, where h is Planck's constant. Experimentally, absorption of power at this frequency is observed.

If the ions are in thermal equilibrium with the crystal lattice, the average numbers of ions found in each state are related by Boltzmann's distribution law

$$n_i/n_j = e^{-(E_i - E_j)/kT_0}. \tag{1}$$

Here k is Boltzmann's constant and T_0 the absolute temperature of the lattice. This distribution is indicated in Fig. 1, where the length of each line representing an energy level is made proportional to its population. The thermal contact between ions and lattice occurs through relaxation processes which, to some degree, may be described by a relaxation time τ_{ij}. This time may be visualized as the average time of ions in state i before relaxing to state j. In thermal equilibrium, as many ions must go from i to j as go in the opposite direction. With the help of (1), we thus find

$$\tau_{ij}/\tau_{ji} = n_i/n_j = e^{-(E_i - E_j)/kT_0}. \tag{2}$$

This equation indicates that the relaxation time is shorter for ions in a higher state. For present purposes, this result as based on Boltzmann theory may be sufficient. It might be mentioned, however, that, following Einstein, the situation of (2) can be described by the concept of spontaneous transitions.[6] These occur only in the downward direction and thereby enhance this relaxation rate. In still another, more modern treatment,[7] the inequality of the two relaxation times in (2) follows directly by taking into account the quantum nature of lattice vibrations or radiation field.

With transitions excited by radiation of frequency ν_{ij}, the rate of transitions is described by the transition probability w_{ij}. The transition probability due to applied radiation is the same for upward and downward transitions, $w_{ij} = w_{ji}$. The energy absorbed from the exciting field is one quantum $h\nu_{ij}$ per transition. The power absorbed per unit volume is therefore

$$P_{ij} = h\nu_{ij}w_{ij}(\rho_j - \rho_i). \tag{3}$$

Here i denotes the higher state and ρ denotes the density of ions in each particular state. Power is emitted rather than absorbed if the densities are "inverted," $\rho_i > \rho_j$.

The transition probability can be written[8]

$$w_{ij} = \frac{1}{4}\left(\frac{2\pi}{h}\right)^2 g(\nu - \nu_{ij}) \mid \mathbf{H}_{rf}^* \cdot \boldsymbol{\mu}_{ij} \mid^2. \tag{4}$$

Here $g(\nu - \nu_{ij})$ is a normalized function describing the line shape as a function of frequency, $\int g(\nu - \nu_{ij})d\nu = 1$; the line is centered at ν_{ij}. $\mathbf{H}_{rf}$ is the exciting rf magnetic field and $\boldsymbol{\mu}_{ij}$ is the magnetic dipole moment associated with the transition from state i to j. Bold face symbols are used to indicate vector (and tensor) quantities. The asterisk (*) denotes the conjugate complex, that is, a quantity having the opposite time dependence. Using Dirac's bracket notation, this dipole moment is defined quantum-theoretically by

$$\boldsymbol{\mu}_{ij} = g\beta \langle j \mid \mathbf{S} \mid i \rangle = \boldsymbol{\mu}_{ji}^*. \tag{5}$$

Here g is the spectroscopic splitting factor, a number usually close to 2, β is the Bohr electronic magneton, $\mathbf{S}$ is the vector spin operator whose components are S_x, S_y and S_z. It should be pointed out that both $\mathbf{H}_{rf}$ and $\boldsymbol{\mu}_{ij}$ are varying in time like $\exp(i\omega_{ij}t)$. This implies the possibility of phase differences between the components of $\boldsymbol{\mu}_{ij}$ or the components of $\mathbf{H}_{rf}$. An important example is that of circular polarization. With respect to some reference system, $\boldsymbol{\mu}_{ij}$ has components μ_x and μ_y equal in am-

plitude but 90° out of phase. Such a transition is excited by the corresponding circularly polarized RF magnetic field, but not by circular polarization of the opposite sense. This property can be used to give nonreciprocal gain and attenuation in the same way as the gyromagnetic behavior of ferrites is utilized in unidirectional passive devices.

Since w_{ij} is proportional to the incident power, the absorption can be described, on a macroscopic scale, by the imaginary part χ'' of susceptibility, where χ'' is independent of power at low power levels. It is a tensor defined by

$$P_{ij} = \tfrac{1}{2}\omega_{ij}\mu_0 \mathbf{H}_{\mathrm{rf}}^* \cdot \chi''_{ij} \cdot \mathbf{H}_{\mathrm{rf}} . \tag{6}$$

By comparison with (3) and (4) we find

$$\mathbf{H}_{\mathrm{rf}}^* \cdot \chi''_{ij} \cdot \mathbf{H}_{\mathrm{rf}} = \frac{\pi}{\mu_0 h}\, g(\nu - \nu_{ij})(\rho_j - \rho_i)\mathbf{H}_{\mathrm{rf}}^* \cdot \mathfrak{y}_{ij}\mathfrak{y}_{ij}^* \cdot \mathbf{H}_{\mathrm{rf}}. \tag{7}$$

This representation shows the tensor character of χ''_{ij}. The properties of the tensor with respect to polarization of $\mathbf{H}_{\mathrm{rf}}$ in space and phase are described by the dyadic product $\mathfrak{y}_{ij}\mathfrak{y}_{ij}^*$. This also shows that this tensor is degenerate. Instead of three nonvanishing eigenvalues it has only one, namely $|\mu_{ij}|^2$ with the associated eigenvector. The eigenvector represents the polarization of the magnetic moment $\mathfrak{y}_{ij}$ with respect to space and phase. Magnitude and polarization of $\mathfrak{y}_{ij}$ in (5) can be calculated in a standard quantum theoretical fashion. Maximum transition probability occurs if $\mathfrak{y}_{ij}$ and $\mathbf{H}_{\mathrm{rf}}$ have the same polarization, which in general will be elliptical.

As an example, we give the numerical values of imaginary part χ'' of susceptibility for a particular transition in ruby.[8] This transition occurs between $-\frac{3}{2}$ and $-\frac{1}{2}$ states (see Fig. 2) at a field of 3.97 kilo-oersted applied perpendicular to the crystalline axis. Its transition frequency is 5.85 kmc. It is the same line whose inversion is discussed below and which is employed in the TWM described in the accompanying paper.[5] We compute the quantities χ''_+ and χ''_-, which are the values of χ'' for excitation with circular polarization. The circular polarization is defined in an x–y plane where the z-direction coincides with the applied dc magnetic field. The magnitude of χ''_+ is defined by

$$|\chi''_+| = (\mathbf{H}_{\mathrm{rf}+}^* \cdot \chi'' \cdot \mathbf{H}_{\mathrm{rf}+})/(\mathbf{H}_{\mathrm{rf}+}^* \cdot \mathbf{H}_{\mathrm{rf}+}) \tag{7a}$$

and similarly for χ''_-.

The ruby crystal is the commercial "pink sapphire" produced by Linde Company. The chromium content of 0.05 per cent substituting for aluminum indicated by the manufacturer was verified by chemical

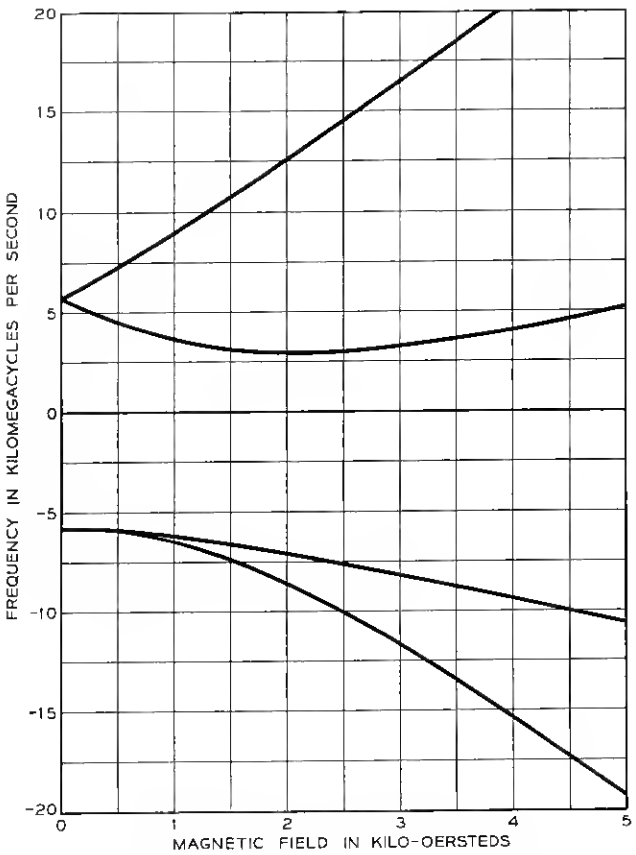

Fig. 2 — Energy-levels of Cr^{+++} in ruby as function of magnetic field applied perpendicular to crystalline symmetry axis.

analysis.[9] We thus have $\rho_0 = 2.35 \times 10^{19}$ Cr^{+++} ions cm^{-3}. For the density difference

$$\rho_{-3/2} - \rho_{-1/2} \approx \frac{\rho_0}{2S+1}\frac{h\nu}{kT}$$

we find, at $T = 1.6°K$, $\rho_{-3/2} - \rho_{-1/2} = 1.04 \times 10^{18}$ cm^{-3}. Assuming a Lorentzian line shape, at the line center $g(0) = 2/\pi\Delta\nu$, where $\Delta\nu = 6 \times 10^7$ sec^{-1} is the measured full line width at half intensity. Using the eigenvectors evaluated in Ref. 8 and (5), we find $|\mu_+|^2 = 5.08 \times 10^{-40}$ erg^2 $oersted^{-2}$ and $|\mu_-|^2 = 0.57 \times 10^{-40}$ erg^2 $oersted^{-2}$. The resulting numbers for susceptibility by circular excitation are $\chi''_+ = 0.0166$ and $\chi''_- = 0.0018$, respectively.

This can be compared with measurements in the TWM which yield $\chi_+''F_+ = 0.0062$, where F_+ is the filling factor for positive circular polarization. By definition, $F_+ < \frac{1}{2}$. We find $F_+ = 0.37$. Since this filling factor is about what should be expected on the basis of TWM geometry, the comparison of the calculated χ_+'' and the measured $\chi_+''F_+$ shows the consistency of experimental data with theoretical computation.

Saturation effects can be discussed considering both relaxation processes and RF excitation present. The population n_i then changes according to

$$\frac{dn_i}{dt} = -\frac{n_i}{\tau_{ij}} + \frac{n_j}{\tau_{ji}} - n_i w_{ij} + n_j w_{ij}. \tag{8}$$

With steady-state conditions, $dn_i/dt = 0$. From this equation, the following features are easily deduced. If the exciting field is weak, $w_{ij}\tau_{ij} \ll 1$, the ratio n_i/n_j is the unperturbed Boltzmann ratio (1). If the exciting field is strong, $w_{ij}\tau_{ij} \gg 1$, saturation occurs; that is, $n_i = n_j$. The Boltzmann difference between n_i and n_j is reduced to half its value with $w_{ij}\tau_{ij} = 1$.

III. THREE-LEVEL EXCITATION

In the three-level maser, a saturating "pump" signal is applied between levels 1 and 3 (see Fig. 1) so that $n_1 \to n_3$. The population n_2 then will be determined by

$$\frac{dn_2}{dt} = -\frac{n_2}{\tau_{21}} - \frac{n_2}{\tau_{23}} + \frac{n_1}{\tau_{12}} + \frac{n_3}{\tau_{32}}.$$

Applying steady state conditions and relations like (2),

$$\frac{n_2}{n_1} = \frac{1 + \dfrac{\tau_{12}}{\tau_{23}}\dfrac{n_3}{n_1}\exp\left(\dfrac{h\nu_{32}}{kT}\right)}{\exp\left(\dfrac{h\nu_{21}}{kT}\right) + \dfrac{\tau_{12}}{\tau_{23}}}, \tag{9}$$

where, with the pump transition saturated, $n_3/n_1 = 1$. Under this condition, the equation indicates that it would be rather accidental if $n_2/n_1 = 1$. If $n_2/n_1 > 1$, stimulated emission could be obtained at ν_{21}. This situation is indicated in Fig. 3. If $n_2/n_1 < 1$, that is, $n_3/n_2 > 1$, maser action could be obtained at ν_{32}.

For further discussion, let us identify arbitrarily ν_{21} *or* ν_{32} with the signal frequency ν_{sig}, and the other frequency with idler frequency ν_{idl}.

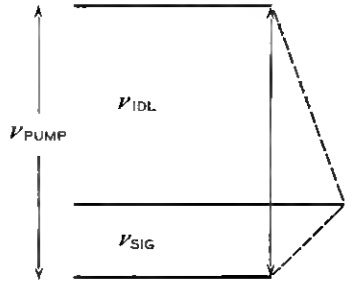

Fig. 3 — Energy-level scheme to demonstrate maser action.

In analogy to (1), we may introduce a spin signal temperature T_{sig} by

$$\frac{n_i}{n_j} = e^{-(h\nu_{sig}/kT_{sig})}, \tag{10}$$

where i is the upper state and j the lower state of the signal transition. Also, we expand the exponential functions in (9) and (10) to the linear term. This is frequently justified under experimental conditions. Even where it is not, the resulting simpler equations show the qualitative features more clearly. We find

$$\frac{T_{sig}}{T_0} = \frac{1 + \dfrac{\tau_{sig}}{\tau_{idl}}}{1 - \dfrac{\tau_{sig}}{\tau_{idl}} \dfrac{\nu_{idl}}{\nu_{sig}}}. \tag{11}$$

We may define as "inversion" the quantity $-T_0/T_{sig}$. It is easily measured in a TWM as the ratio of gain with saturating pump power to attenuation without pump power, both expressed in decibels. To obtain large gain and bandwidth from a given number of ions in a crystal at T_0, the inversion should be as large as possible or the negative T_{sig} should be as small as possible. This suggests that it would be desirable for

$$\tau_{sig}/\tau_{idl} \gg 1 \tag{12}$$

and

$$\nu_{idl}/\nu_{sig} \gg 1, \tag{13}$$

In most experiments performed up to now, however, maser action was based on one of these ratios being large, while the other was not appreciably different from unity. Consequently, it is convenient to distinguish between "relaxation time ratio operation" of 3LSSM, where (12) is satisfied, and "frequency ratio operation", where (13) is satisfied. Both modes of operation will be discussed in more detail below.

Before entering this discussion, however, let us now consider two interesting refinements of (11). The first is concerned with saturation of the signal transition. It will determine the upper limit of the dynamic range of a maser amplifier. For this, a transition probability w_{sig} at the signal frequency ν_{sig} is introduced. Instead of (11) we then find

$$\frac{T_{sig}}{T_0} = \frac{\left(1 + \frac{\tau_{sig}}{\tau_{idl}}\right)\left(1 + w_{sig}\frac{\tau_{sig}\tau_{idl}}{\tau_{sig} + \tau_{idl}}\right)}{1 - \frac{\tau_{sig}}{\tau_{idl}}\frac{\nu_{idl}}{\nu_{sig}}}. \tag{14}$$

The numerator shows that, in saturating a maser signal, the applied RF field has to overcome the shunted signal and idler relaxation times. Thus, in general, the maser signal saturates at a higher power level than the same line in the absorbing state. If both relaxation times are appreciably different, this shunted value is essentially the shorter of the two. The difference in saturation levels is drastic, therefore, if the idler relaxation time is short compared to the signal relaxation time.

The other refinement considered is the effect of incomplete saturation of the pump transition. Such considerations are important with the application of very high pump frequencies. For a description of incomplete saturation, a pump temperature T_{pump} is defined analogously to the signal temperature in (10). The resulting modification of (11) is

$$\frac{T_{sig}}{T_0} = \frac{1 + \frac{\tau_{sig}}{\tau_{idl}}}{1 - \frac{\tau_{sig}}{\tau_{idl}}\frac{\nu_{idl}}{\nu_{sig}}\left(1 - \frac{\nu_{pump}}{\nu_{idl}}\frac{T_0}{T_{pump}}\right)}. \tag{15}$$

The denominator shows that, with comparatively high pump frequencies, appreciable inversion can be achieved with slight saturation of the pump transition. Suppose a certain inversion results from complete saturation ($T_{pump} \rightarrow \infty$) at pump frequency ν_{pump}. With the relaxation time ratio unchanged, the same inversion occurs with pump frequency $\nu'_{pump} = a\nu_{pump}$ (a is a number greater than unity) and pump temperature $T'_{pump} =$

$aT_0/(a-1)$. For example, with $\nu'_{\text{pump}} = 2\ \nu_{\text{pump}}$, this requires $T'_{\text{pump}} = 2\ T_0$. In this sense, pump frequency can be traded for pump saturation.

IV. RELAXATION TIME RATIO OPERATION

We have defined this operation by $\tau_{\text{sig}}/\tau_{\text{idl}} \gg 1$, while $\nu_{\text{idl}}/\nu_{\text{sig}}$ is not specified but not too far from unity. From (11), we thus find

$$T_{\text{sig}}/T_0 = -\nu_{\text{sig}}/\nu_{\text{idl}}\,. \tag{16}$$

Following the discussion of (14), a particularly attractive property of this operation is that the inverted signal transition saturates at a rather high power level in proportion to the idler relaxation time. By the same token, after a very strong signal resulting in saturation of the signal transition, the amplifying condition is restored in a short time, of the order of the idler relaxation time.

Unfortunately, experimental data about relaxation times are rather scarce. Usually, our experiments have yielded relaxation time ratios close to one; only in exceptions have they been as high as five. Also, there is no adequate theory of relaxation processes that would enable one to compute conditions leading to large relaxation time ratios. This difficulty was bypassed by Scovil and Feher using a technique of impurity doping.[2] We explain this technique by considering the effect of concentration on relaxation times.

At very low concentrations, ions do not interact with each other. The individual resonance lines are narrow, but slightly displaced with respect to each other, as a result of random local fields. The observed over-all line is "inhomogeneously" broadened.[10] In this range, line width and relaxation time should be independent of concentration. With higher concentration, spin-spin interaction comes into play in two ways: (a) the dc magnetic field associated with neighboring spins produces addition inhomogeneous broadening; (b) the RF magnetic field associated with spins during relaxation type transitions leads to "homogeneous" broadening in excess of the inhomogeneous. This can be visualized as a resonant coupling between spins which results in a broader line of identical frequency for every ion. The homogeneous broadening increases proportionally to ion concentration. Gadolinium ethyl sulfate as a maser material is used in a range where homogeneous broadening outweighs the inhomogeneous broadening effects by about a factor of two. This is the case with a concentration of 0.5 per cent gadolinium in a diamagnetic

host crystal of lanthanum ethyl sulfate. Some measurements in this concentration range in our laboratory have indicated a rather strong dependence of relaxation time on concentration. A typical value found is a reduction in relaxation time by a factor of 10 upon doubling the ion concentration. This applies to the pump relaxation time, too, indicating a rather strong concentration dependence of pump power required to saturate the pump transition. In practice, one uses as high an ion concentration as is compatible with the pump power which is available and which can be dissipated in the cryostat, in order to have maximum gain and bandwidth per volume of maser material.

In the doping technique, an additional transition is used, whose frequency coincides with that of the idler transition and whose dipole moment is similar to that of the idler. Spin-spin interaction will then be effective at the idler frequency, which can be regarded as due to an effective increase of ion concentration. As a result, the idler relaxation time is shortened considerably. On the basis of the figure given above, a reduction in relaxation time by a factor of 10 might be expected for an effective doubling of ions in the idler transition. It should be pointed out, however, that at lower ion concentrations such as are typical of inhomogeneous broadening, no doping effects are observed. In this range, the idler relaxation time is essentially unaffected by the doping transition.

The doping transition may be one between other levels in the same ion energy level scheme. We call this case "self-doping condition." Alternatively, the doping condition can be provided by a transition of another ion spectrum within the same crystal lattice. This case we call "impurity doping condition." An advantage of this latter case is the free choice of impurity concentration which allows one to control the strength of doping action.

We will illustrate this type of operation by describing the use of gadolinium in a crystal of hydrated lanthanum ethyl sulfate containing cerium as an additional impurity. Fig. 4 shows part of a measured spectrum of a crystal containing 0.5 per cent gadolinium and 0.2 per cent cerium. Resonance fields for a signal frequency of 6.298 kmc are plotted versus the angle between applied magnetic field and crystalline axis. Experimentally, doping conditions are found at crossover points of lines in an observed spectrum. The energy-level diagrams indicating the doping conditions at points A and B in Fig. 4 are shown in Fig. 5. Relaxation times were measured by the saturation method. With uncluttered $-\frac{3}{2} \leftrightarrow -\frac{1}{2}$ and $-\frac{1}{2} \leftrightarrow +\frac{1}{2}$ lines, the relaxation times are nearly the same. At point A, the $-\frac{1}{2} \leftrightarrow +\frac{1}{2}$ relaxation time τ_{1a1} is reduced by a factor of 5. The effect is comparatively small because the $+\frac{5}{2}$ and $+\frac{7}{2}$

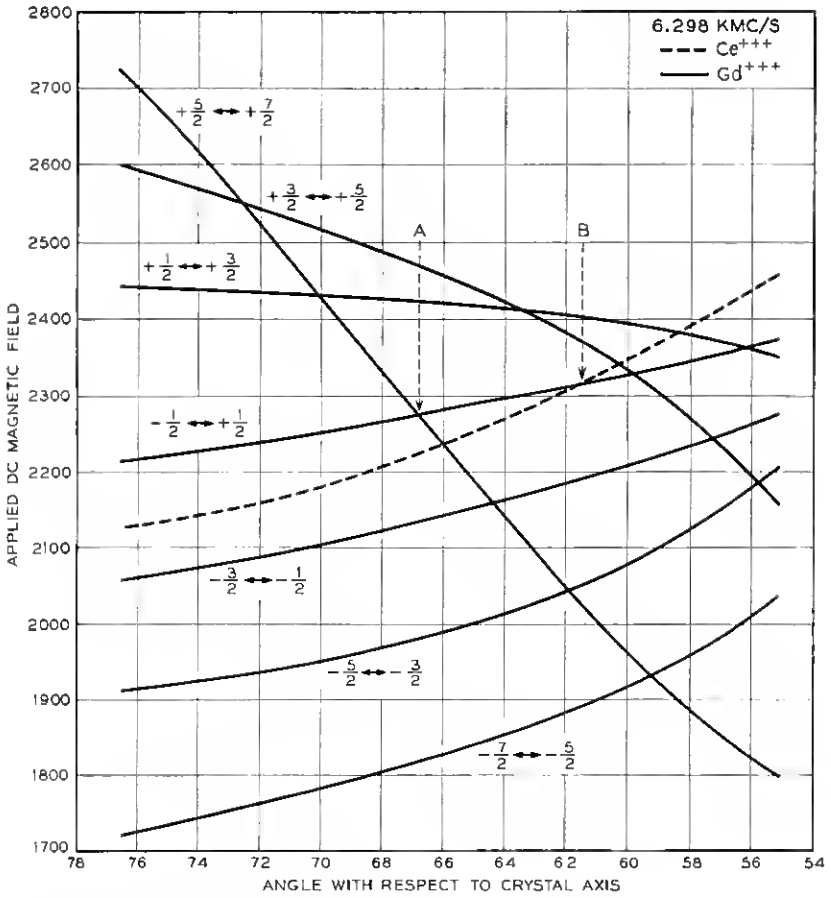

Fig. 4 — Part of measured paramagnetic resonance spectrum of lanthanum ethyl sulfate containing gadolinium and cerium.

levels are not very populated at 1.5°K. As should be expected from (11) with a frequency ratio $\nu_{idl}/\nu_{sig} = 0.94$, the measured inversion obtained by applying pump power to the $-\frac{3}{2} \leftrightarrow +\frac{1}{2}$ transition was $-T_0/T_{sig} = 0.5$. At point B, reduction in τ_{idl} was by a factor 10. In agreement with this, inversion observed was $-T_0/T_{sig} = 0.8$. Possibly the near crossover of $+\frac{3}{2} \leftrightarrow +\frac{5}{2}$ is helpful in achieving the large reduction of τ_{idl}. For it was found that strong doping was effective even when idler and doping frequency differed by as much as 100 mc, i.e., more than the line width (30 mc). Further tests showed saturation of the inverted signal at about 10 times the saturating power required for the absorption sig-

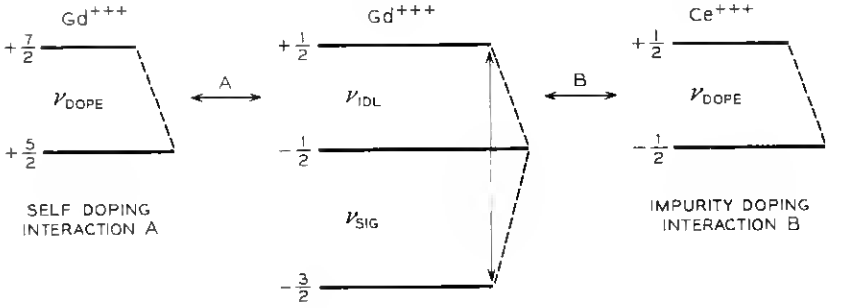

Fig. 5 — Energy-level scheme to describe self- and impurity-doping conditions

nal. In our slow-wave structure, the respective power levels were 32 mw and 3.2 mw. After a complete saturation, the amplification is restored to within $\frac{1}{8}$ of its steady-state value within 20 microseconds indicating $\tau_{id1} \approx 10$ microseconds. The signal transition is almost completely circular. Thus, the degree of nonreciprocity in gain is limited by the perfection of the microwave structure only. In a test slow-wave structure exhibiting a slowing of 100 compared to velocity of light, essentially unidirectional gain of 4.5 db/cm was obtained.

While this material shows appreciable power-handling capacity and fast recovery, it is not too well suited for practical application because of chemical instability and mechanical weakness. Somewhat disadvantageous, too, is the low pump-transition probability at the frequencies used in our experiments, which has to be overcome by high pump fields. Also, because of nearly equal level spacing, $\nu_{id1}/\nu_{sig} \approx 1$ and inversion will be limited to order 1. These disadvantages are avoided by the use of ruby at the expense of somewhat lower gain, lower signal saturation and slower recovery.

V. FREQUENCY RATIO OPERATION

Equation (11) suggests that inversion can always be achieved by a sufficiently large ratio ν_{id1}/ν_{sig} independent of τ_{sig}/τ_{id1}. From a practical point of view, there are limits to this approach. For a given signal frequency, the highest useful ratio ν_{id1}/ν_{sig} is restricted by pump power sources available at high microwave frequencies. Depending on the power requirements, this limit lies presently between perhaps 35 and 100 kmc, unless optical, incoherent power sources could be utilized. Also, one would like to use for practical masers only such operations where the

relaxation time ratio τ_{sig}/τ_{idl} is at least not below unity. If this is satisfied, one might expect an inversion of order

$$-T_0/T_{sig} \approx \nu_{idl}/2\nu_{sig} . \tag{17}$$

The inversion could be improved with a more favorable relaxation time ratio.

For our experiments with frequency ratio operation at low signal frequencies, the energy-level diagram of ruby[8, 11, 12] was used with magnetic field applied perpendicular to the crystalline symmetry axis. This diagram is shown in Fig. 2. Use of the perpendicular orientation is suggested by the observation that all lines are reasonably narrow (of order 60 mc in 0.05 per cent ruby) and correspondingly intense at this orientation and that all possible transitions are reasonably probable. For a signal frequency of about 5.8 kmc, two transitions are available. One is between $+\frac{1}{2}$ and $+\frac{3}{2}$ levels at about 1.0 kilogauss. With a pump frequency of about 15 kmc between either $-\frac{3}{2}$ or $-\frac{1}{2}$ and $+\frac{3}{2}$, no inversion was observed but only saturation of the signal. This indicates an unfavorable relaxation time ratio of about $\tau_{sig}/\tau_{idl} = 0.7$. The other signal transition occurs between $-\frac{3}{2}$ and $-\frac{1}{2}$ levels at a field of 3.97 kilogauss. The $-\frac{3}{2} \leftrightarrow +\frac{1}{2}$ transition is used for pumping at a frequency of about 18.5 kmc. The inversion found is $-T_0/T_{sig} = 0.95$. Thus, the relaxation time ratio $\tau_{sig}/\tau_{idl} = 1.45$ favors this maser operation.

Both relaxation times are rather long, of the order $\frac{1}{10}$ second. Consequently, gain saturation at the output sets in at a fairly low level of 6 microwatts c.w. output power in our structure. The power level of saturation can be appreciably higher in pulsed operation. This can be understood by considering the energy stored in the inverted spin system. As long as pulses repeat in a time shorter than the relaxation time, it is only the average power which determines the saturation behavior. Thus, with a 10^{-3} duty cycle, saturation was observed at peak power of 6 mw.

VI. OPTIMIZATION OF MASER MATERIAL OPERATION

From the preceding discussion, it is apparent that the distinction of relaxation time ratio operation and frequency ratio operation is somewhat artificial. This classification is justified, however, because both cases offer viewpoints for the experimental approach to maser operation. They allow one to predict maser action with a reasonable chance of success from the knowledge of the energy-level diagram only. In the relaxation time ratio operation, the respective ion concentrations are the only critical parameters whose effect has to be investigated experimen-

tally. They have to be compatible with the doping effect and pump power available. In the frequency ratio operation, similarly, maser action is assured if the line is homogeneously broadened, if the pump power available is sufficient for saturation and if the relaxation time ratio is not too unfavorable. It is clear that an ideal maser material should exhibit both a large frequency ratio ν_{idl}/ν_{sig} within practical limits set by available pump power sources *and* a large relaxation time ratio τ_{sig}/τ_{idl}. To accomplish the first, paramagnetic materials with high zero field splitting are required. To accomplish the second, another similar spectrum of a different ion or ion site within the same host crystal could be used for doping the idler relaxation time. This approach requires a rather intimate knowledge of the involved paramagnetic spectra, but there is little doubt that more ideal maser materials will be found as development continues.

VII. NONRECIPROCAL ATTENUATION

The development of unilateral TWM depends on the availability of elements exhibiting nonreciprocal attenuation. In contrast to conventional ferrite nonreciprocal devices, which operate at room temperature and at a magnetic field adjusted for optimum performance of the device, the nonreciprocal behavior in the TWM must be achieved at a low temperature and at a field dictated by the maser operation. Two practical solutions have been found so far, while others may appear useful in the future.

The first approach uses the same paramagnetic material as that supplying maser gain, but with positive signal temperature. Experimentally it was established that the pump power used in the ruby TWM (of order 100 mw) is not sufficient to saturate the pump transition of a higher concentration (0.9 per cent) ruby. At the signal frequency, only very slight reduction in attenuation was observed. Thus it is possible to place low- and high-concentration materials together into the same structure, with one exhibiting gain and the other attenuation. Suppose a forward wave in the structure produces right circular polarization in one region, left circular in another. Both gain and isolator materials interact with right circular polarization only. Thus, we place gain material in the right circular region so that it amplifies the forward wave. Isolator material in the left circular region does not interact with the forward wave. A reverse wave, however, produces the opposite senses of circular polarization. This can easily be verified by the observation that, aside from absorption, a reversal of direction of propagation is equivalent to a

change in sign of time. Thus, the right circular polarization of the reverse wave interacts with the isolator material, but not with the gain material. Ideally, pure forward gain and pure reverse attenuation should result. In practice, the reverse-to-forward ratio of attenuation has an upper limit, C, the circularity of the signal transition, which then will be further reduced by variation of the degree of circular polarization in the microwave structure. The same applies to the forward-to-reverse ratio of gain. For the ruby signal transition discussed before, $C = |\chi''_+|/|\chi''_-| = 8.95$.

One obvious advantage of using the same paramagnetic ion for amplification and for isolation is that the resonance condition will always occur at the same magnetic field. The isolator will automatically track the amplifying material with electronic tuning. One disadvantage is that pump power will be absorbed by the isolator. It is not saturated at the pump frequency and therefore absorbs a major fraction of the pump power.

This difficulty could be avoided by using a different paramagnetic material as isolator. In practice, this approach may be rather difficult because the resonance line considered should occur at a magnetic field given by the maser operation and, in addition, it should exhibit high circularity.

The other approach is to use ferrimagnetic materials. Investigations on the resonance behavior of ferrimagnetic materials at liquid helium temperature are being carried out by F. W. Ostermayer of Bell Telephone Laboratories. While he shall report his results in detail, we mention some typical features. Three ferrimagnetic polycrystalline materials have shown useful resonance properties at helium temperature. They are yttrium iron garnet, yttrium gallium iron garnet and nickel zinc ferrispinel. From a room temperature line width usually below 50 oersteds, the helium temperature line width is of the order of 1000 oersteds for these materials. The strength of the resonance absorption decreases accordingly. Still, the resonance absorption is very strong compared to gain or attenuation due to paramagnetics. Therefore the ferrite volumes used in a TWM are extremely small. The resonance field can be shifted to the field required for the maser action within a range set by the saturation magnetization by shaping the ferrite sample. The shape follows from the demagnetizing factors, which in turn are calculated from Kittel's[13] resonance condition.

Two such isolators have been tested as parts of a TWM. One used 0.020-inch diameter spheres of yttrium gallium iron garnet and was used in conjunction with the maser operation of gadolinium ethyl sul-

fate described before. The applied field of about 2.1 kilogauss provided resonance conditions for both the active material and the isolator. Reverse-to-forward attenuation at helium temperature was better than 30. The other is a rectangular slab of nickel zinc ferrispinel with 0.010- by 0.020-inch cross section having the length of the maser slow wave structure. Its resonance field is sufficiently close to that of the $-\frac{3}{2}$ to $-\frac{1}{2}$ line in ruby at 5.85 kmc and with crystalline symmetry axis perpendicular to the applied magnetic field. Maser operation using this line is described above. At helium temperature, the ratio of reverse to forward attenuation in the nickel zinc ferrispinel isolator is better than 10. In both cases, the isolator reverse attenuation is adjusted to exceed the forward maser gain slightly. Due to the large ferrimagnetic line width, no great care has to be taken to have the maser magnetic field coincident with the field of the resonance isolator. By the same token, tracking over reasonably wide bands by electronic tuning is not difficult. A decisive advantage of ferrimagnetic isolation is the small interaction of the ferrimagnetic material with the pump frequency. Also, the figure of merit favors this type of isolation, so that it appears as the more attractive possibility.

VIII. SUMMARY

The use of active materials in three-level solid state masers has been discussed. Experimental data have been presented for two typical paramagnetic salts used as active materials in masers. Maser action in these materials can be analyzed in terms of two important modes of operation that make use of either a favorable ratio of signal to idler relaxation time or a favorable ratio of idler to signal frequency. It has been pointed out that more ideal maser materials can be developed that combine the advantages of both modes of operation. Some mention has been made of the use of paramagnetic and ferrimagnetic materials for low-temperature isolators. While the experimental results warrant the use of some materials presently available in practical traveling-wave masers, appreciably improved characteristics can be expected from better materials yet to be developed. The application of active and isolator materials to a traveling-wave maser is treated in the accompanying paper.

REFERENCES

1. Bloembergen, N., Proposal for a New-Type Solid State Maser, Phys. Rev., **104**, October 1956, p. 324.
2. Scovil, H. E. D., Feher, G. and Seidel, H., Operation of a Solid State Maser, Phys. Rev., **105**, January 1957, p. 762.
3. McWhorter, A. L. and Meyer, J. W., Solid State Maser Amplifier, Phys. Rev., **109**, January 15, 1958, p. 312.

4. Makhov, G., Kikuchi, C., Lambe, J. and Terhune, R. W., Maser Action in Ruby, Phys. Rev., **109**, February 15, 1958, p. 1399.
5. DeGrasse, R. W., Schulz-DuBois, E. O. and Scovil, H. E. D., this issue, p. 305.
6. Einstein, A., Phys. Zeit, **18**, 1917, p. 121.
7. Fermi, E., Rev. Mod. Phys., **4**, 1932, p. 87; Rosenfeld, L., Ann. Inst. Henri Poincare, **1**, 1931, p. 25; Heitler, W., *Quantum Theory of Radiation*, 2nd Ed., Oxford Univ. Press, New York, 1944.
8. Schulz-DuBois, E. O., Paramagnetic Spectra of Substituted Sapphire—Part I: Ruby, B.S.T.J., **38**, January 1959, p. 271.
9. Wood, D. L., private communication.
10. Portis, A. M., Phys. Rev., **91**, 1953, p. 1071.
11. Manenkov, A. A. and Prokhorov, A. M., J. Exp. Theor. Phys. (U.S.S.R.), **28**, 1955, p. 762.
12. Geusic, J. E., Phys. Rev., **102**, 1956, p. 1252.
13. Kittel, C., Phys. Rev., **71**, 1947, p. 270.